IL-1α induces thrombopoiesis through megakaryocyte rupture in response to acute platelet needs

Satoshi Nishimura,[1,2,5,6] Mika Nagasaki,[1,3] Shinji Kunishima,[7] Akira Sawaguchi,[8] Asuka Sakata,[5] Hiroyasu Sakaguchi,[9] Tsukasa Ohmori,[5] Ichiro Manabe,[1] Joseph E. Italiano Jr.,[10] Tomiko Ryu,[11] Naoya Takayama,[12] Issei Komuro,[1,2] Takashi Kadowaki,[2,4] Koji Eto,[12] and Ryozo Nagai[5]

[1]Department of Cardiovascular Medicine, [2]Translational Systems Biology and Medicine Initiative, [3]Computational Diagnostic Radiology and Preventive Medicine, [4]Department of Diabetes and Metabolic Diseases, The University of Tokyo, Tokyo 113-8654, Japan
[5]Center for Molecular Medicine, Jichi Medical University, Tochigi 329-0498, Japan
[6]Japan Science and Technology Agency (JST), Precursory Research for Embryonic Science and Technology (PRESTO), Saitama 332-0012, Japan
[7]Department of Advanced Diagnosis, Clinical Research Center, National Hospital Organization Nagoya Medical Center, Nagoya 460-001, Japan
[8]Department of Anatomy, Ultrastructural Cell Biology, Faculty of Medicine, University of Miyazaki, Miyazaki 889-1692, Japan
[9]Web Solution Group, IMAGICA Imageworks, Tokyo 141-0022, Japan
[10]Division of Hematology, Department of Medicine, Brigham and Women's Hospital, Vascular Biology Program at Boston Children's Hospital, Harvard Medical School, Boston, MA 02215
[11]Internal medicine, Social Insurance Central General Hospital, Tokyo 105-8330, Japan
[12]Center for iPS Cell Research and Application, Kyoto University, Kyoto 606-8507, Japan

Intravital visualization of thrombopoiesis revealed that formation of proplatelets, which are cytoplasmic protrusions in bone marrow megakaryocytes (MKs), is dominant in the steady state. However, it was unclear whether this is the only path to platelet biogenesis. We have identified an alternative MK rupture, which entails rapid cytoplasmic fragmentation and release of much larger numbers of platelets, primarily into blood vessels, which is morphologically and temporally different than typical FasL-induced apoptosis. Serum levels of the inflammatory cytokine IL-1α were acutely elevated after platelet loss or administration of an inflammatory stimulus to mice, whereas the MK-regulator thrombopoietin (TPO) was not elevated. Moreover, IL-1α administration rapidly induced MK rupture–dependent thrombopoiesis and increased platelet counts. IL-1α–IL-1R1 signaling activated caspase-3, which reduced plasma membrane stability and appeared to inhibit regulated tubulin expression and proplatelet formation, and ultimately led to MK rupture. Collectively, it appears the balance between TPO and IL-1α determines the MK cellular programming for thrombopoiesis in response to acute and chronic platelet needs.

Introduction

Circulating platelet counts and thrombopoietic processes in BM megakaryocytes (MKs) are both tightly regulated. In vitro, thrombopoiesis occurs via proplatelet formation (PPF) in the presence of thrombopoietin (TPO), which entails microtubule-dependent extension of elongated pseudopodal structures that exhibit platelet-sized swellings arranged in tandem and containing platelet organelles (Patel et al., 2005; Thon et al., 2010; Machlus et al., 2014). In vivo studies using two-photon microscopy also confirmed the presence of PPF in mouse BM (Junt et al., 2007; Zhang et al., 2012). However, the estimated platelet number released from each MK cannot explain rapid platelet turnover, especially when the need is acute, such as during inflammatory reactions. We therefore suspected that there is another rapid thrombopoietic mode, in addition to PPF.

Although TPO has been identified as the most important regulator of platelet production (de Sauvage et al., 1994; Kuter, 2007), it was recently reported that MK maturation and platelet biogenesis can occur independently of TPO (Ng et al., 2014).

Correspondence to Satoshi Nishimura: snishi-tky@umin.ac.jp; or Koji Eto: kojieto@cira.kyoto-u.ac.jp

Abbreviations used in this paper: FRAP, fluorescent recovery after photobleaching; HSC, hematopoietic stem cell; MK, megakaryocyte; PPF, proplatelet formation; ROI, region of interest; TPO, thrombopoietin.

© 2015 Nishimura et al. This article is distributed under the terms of an Attribution–Noncommercial–Share Alike–No Mirror Sites license for the first six months after the publication date (see http://www.rupress.org/terms). After six months it is available under a Creative Commons License (Attribution–Noncommercial–Share Alike 3.0 Unported license, as described at http://creativecommons.org/licenses/by-nc-sa/3.0/).

The Rockefeller University Press $30.00
J. Cell Biol. Vol. 209 No. 3 453–466
www.jcb.org/cgi/doi/10.1083/jcb.201410052

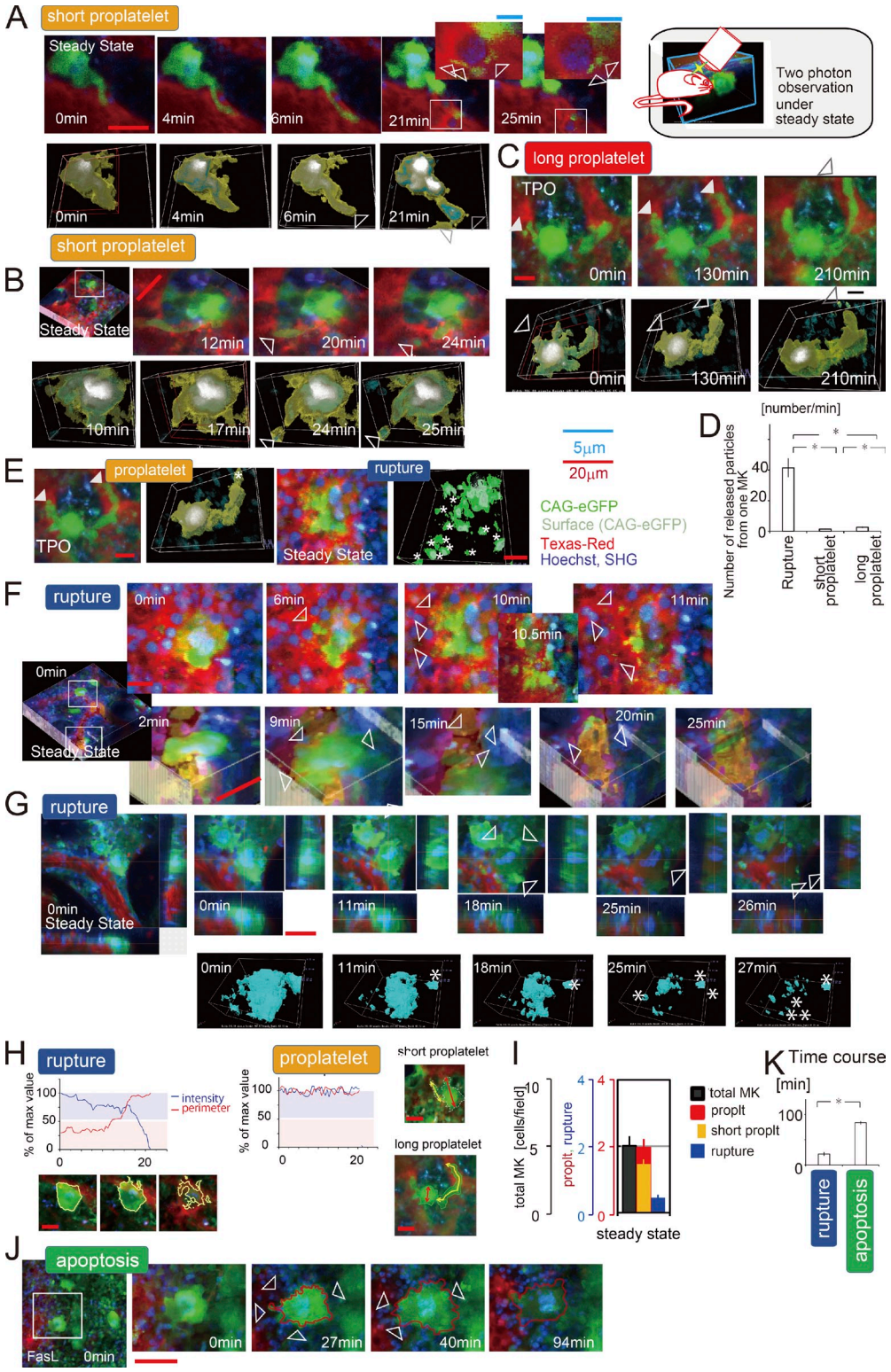

Figure 1. **Proplatelet formation is the dominant mode of thrombopoiesis, but there is an alternative megakaryocyte rupture mode, which produces much larger numbers of platelet-like particles.** (A–G) Time-lapse images of thrombopoiesis in living BM from 6-wk-old CAG-eGFP (green) mice under steady-state conditions (A, B, F, and G) or after treatment with TPO (C; 10 µg for 5 d; A, Video 1; B, Video 2; C, Video 3; F, Videos 4 and 5; and G, Video 6). Injected fluorescent dextran (red) shows the blood flow, and Hoechst (blue) labeled the nucleus. Slice views (top in A, C, and G), voxel views (bottom in B and F), and surface views (bottom row in A, B, C, and G) show MK surfaces and particle release at the single-platelet (triangle) level. (D and E) Numbers of particles released from MKs with proplatelet formation and MK rupture thrombopoiesis, which were calculated from visuals by automatic software. $n = 50$ cells from 5 animals in each group. Note that MK rupture thrombopoiesis is rapid and associated with much greater numbers of released particles. (H) Automatic software analysis of thrombopoiesis mode. Calculated changes in MK perimeters and cytoplasmic GFP signal intensities are shown. The long arm projections (>50% of the length of the mean MK diameter) were identified as proplatelets and divided into short (<100 µm) and long (>100 µm) proplatelet formation. Increases in the perimeter (deformity) and decreases in GFP intensity (during rupture) were identified as the MK rupture pattern.

However, no suggestions as to the detailed mechanism by which platelets are generated from MKs in the absence of TPO were provided. In addition, recent studies indicate that hematopoietic stem cells (HSCs) and MKs are in very close proximity within the hematopoiesis hierarchy, and that MKs and platelets can emerge directly from HSCs under stress conditions, e.g., after BM suppression by irradiation (Sanjuan-Pla et al., 2013; Yamamoto et al., 2013; Nakamura-Ishizu et al., 2014). Thus, the actual pathways of platelet biogenesis are not clear, and elucidation of unidentified thrombopoietic mechanisms, particularly under stressful conditions such as inflammation or acute thrombocytopenia, require direct visualization of the BM. We therefore endeavored to improve the capability of the two-photon microscopy technique such that we would be able to visualize platelet biogenesis from MKs at the single-platelet level and to trace the translocation of platelets into the blood circulation of the BM in living mice. Ultimately, we identified an alternative pathway entailing MK rupture–enhanced platelet release, which responded to acute platelet needs under regulation by IL-1α. Our results shed light on what appears to be a novel mode of platelet release from BM MKs.

Results

Proplatelet type thrombopoiesis continuously regulates the platelet supply but provides limited numbers of platelets from mature MKs

To address the mechanism by which rapid platelet turnover is regulated, especially under stress conditions, we visualized megakaryopoiesis and dynamic thrombopoiesis in three dimensions (3D) using an improved intravital visualization technique and focusing on BM MKs. The combined technologies of multicolor high-sensitivity GaAs detectors, resonance mirror high-speed scanners, and a piezo-drive electronically controlled stage were applied to CAG-eGFP and CD41-tandem(td)Tomato mice, enabling us to monitor the behavior of single platelets shed from BM MKs (Fig. 1, A–C; Fig. S1; and Videos 1–3). MKs identified based on their large size, multinucleation, CD41 positivity, and strong GFP signals in CAG-eGFP mice were mainly located in the border area between BM vessel lumens and the stroma.

With no intervention under steady-state conditions, filamentous (elongated) proplatelets released small platelet-like particles from the tips of the protrusions within vessels (Fig. 1, A and B). The entire time course of this process was usually longer than the observation periods (1 h), during which release was intermittent, and the number of released particles was only 1.4 ± 0.3 per minute from a single MK. TPO administration increased PPF with development of longer (>100 µm) arm projections, but the numbers of released platelets (2.6 ± 0.5 per minute) were still small (Fig. 1, C and D), which prompted us to search for alternative modes of thrombopoiesis.

MK rupture, the alternative mode of thrombopoiesis, can release large numbers of platelets over a short period

Rigorous 3D and high-speed examinations and surface visualization revealed that there is another, minor, but distinct, mode of thrombopoiesis, which we named "MK rupture" thrombopoiesis (Fig. 1, D–G). During the rupture phenomenon, MKs exhibited ruffling and then irregular changes in cell shape, and GFP^+ platelet-like particles were released from the cytoplasm primarily into BM vessel lumens (Fig. 1, F and G; and Videos 4–6). Thereafter, MKs showed a marked loss of the GFP signal from the cytoplasm along with an increase in the dextran signal. When we profiled the visuals of the thrombopoiesis process in MKs using automatic, software-based algorithms, we found that short PPF was the dominant mode of platelet biogenesis in the steady state (Fig. 1, H and I), but that MK rupture thrombopoiesis also occurred with increased particle number per a single MK (Fig. 1 D). Moreover, the MK rupture thrombopoiesis was distinct from typical FasL-induced apoptosis, which had a much longer time course and was associated with blebbing, large protrusions, and gradual GFP loss (Fig. 1, J and K).

MK rupture increases in response to acute platelet needs

We also found that MK rupture–dependent platelet formation increased after intraperitoneal administration of anti-CD42b blocking antibody, which induces acute platelet loss, or thioglycolate, which induces innate inflammation (Fig. 2, A–C; and Video 7). This suggests that the MK rupture phenomenon mediates rapid platelet release in response to acute platelet demand.

IL-1α contributes to MK rupture thrombopoiesis in response to acute platelet need

To determine whether TPO is involved in MK rupture thrombopoiesis, or whether other intrinsic factors are involved, we next sought mediators in BM cell culture medium that positively influenced MK production in the presence of TPO. Using this screening assay, we identified seven candidate factors and determined that IL-1α increases platelet production from MKs to an even greater degree than TPO (Fig. 3, A and B). Moreover, serum IL-1α levels were acutely increased during platelet recovery after depletion using an anti-CD42b antibody, whereas increases in TPO levels were not seen until day 7 (Fig. 3 C). Increases in serum IL-1α levels induced in response to acute peritoneal inflammation evoked by thioglycolate injection were accompanied by transient increases in platelets (Fig. 3 D). In addition, neutralizing anti–IL-1 receptor (IL-1R) antibody

The data shown are from a single representative experiment from among more than five cells from different animals. (I) MK dynamics in 6-wk-old CAG-eGFP mice. Short type proplatelet was dominant in the steady state. n = 50 HPFs from 5 animals in each group. *, $P < 0.05$ versus control mice. (J) Time-lapse images of FasL-induced apoptosis (5 µg/mouse, i.v.). Note that the entire time course was relatively slow, and was not associated with particle release. (K) Time duration of the MK rupture and proplatelet processes. The onset is defined as the increase in perimeter (irregularity), and the end as the loss of GFP intensity (cell death). n = 15 MKs from steady-state (for MK rupture) and FasL-treated mice (for apoptosis). Bars: (red) 20 µm; (blue) 5 µm.

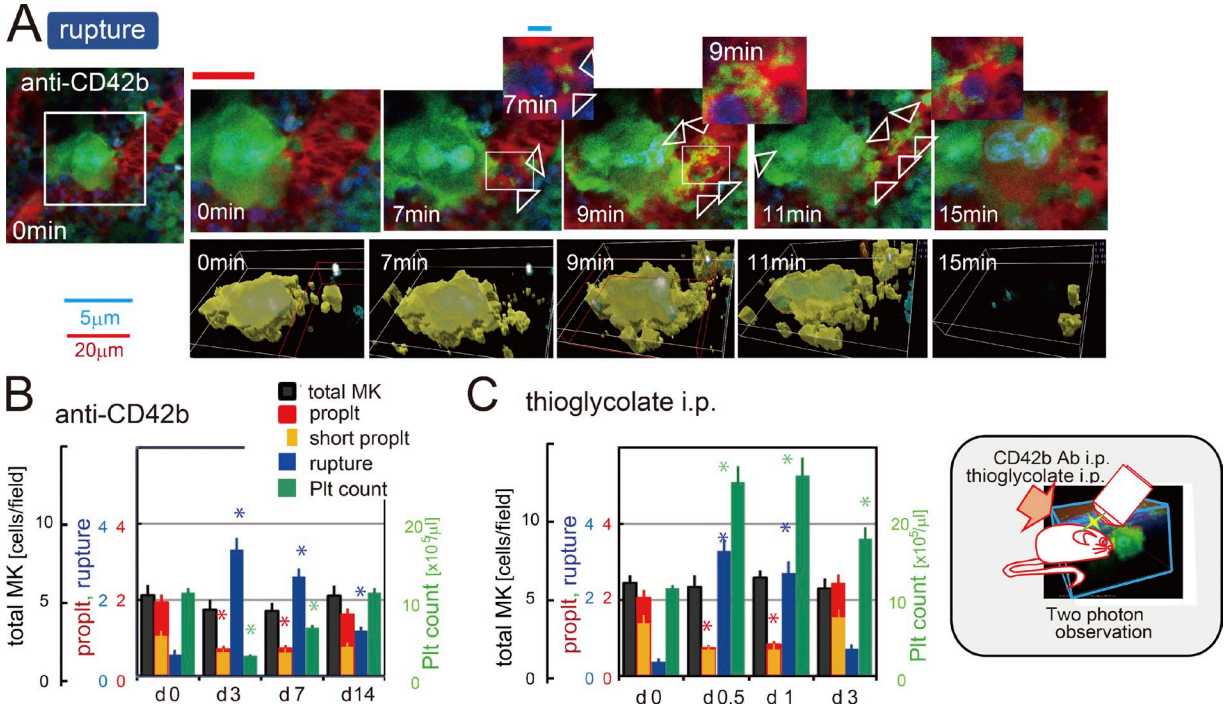

Figure 2. **MK rupture thrombopoiesis responds to acute platelet needs.** (A) Time-lapse image of MK rupture mode thrombopoiesis in MKs in 6-wk-old CAG-eGFP mice after administration of a neutralizing anti-CD42b antibody (100 µg/mouse i.p. daily for 3 d; Video 7). (B and C) Platelet counts and MK dynamics in 6-wk-old CAG-eGFP mice treated with anti-CD42b antibody (B) or with thioglycolate, which induces acute peritoneal inflammation (C). *n* = 8 animals in each group. Bars: (red) 20 µm; (blue) 5 µm. *, P < 0.05 versus day 0.

diminished the platelet response by half and suppressed MK rupture (Fig. 3 E). These results indicate a direct contribution of IL-1α to acute thrombopoietic responses in MKs.

IL-1α induced MK rupture thrombopoiesis in BM MKs

When we further analyzed the effect of exogenous IL-1α on BM MK dynamics in vivo, we found that it markedly increased MK rupture but significantly decreased PPF without changing serum TPO levels (Fig. 4, A–D; Fig. S2; and Videos 8–10). Software analysis showed that the released particle number was 41.5 ± 6.3 per min from each ruptured MK, which is 20 times higher than that achieved with PPF (Fig. 1 D). Circulating platelet counts rapidly increased from day 1 onward, with transient reduction and following increase in MK numbers, but the effects of TPO on platelet counts were only seen at later times (Fig. 4, E–G). Conversely, platelet counts were reduced by a neutralizing anti–IL-1α or anti–IL-1R antibody. This action of IL-1α promoting MK rupture thrombopoiesis was dependent on the IL-1α–IL-1R1 signaling axis, which was confirmed using IL-1α$^{-/-}$ CAG-eGFP and IL-1R1$^{-/-}$ CAG-eGFP mice (Fig. 4 H and Fig. S2), as well as in BM transplantation experiments (Fig. 4 I).

Platelets released from IL-1α–treated MKs are larger in size but show normal function

Using thiazole orange staining to detect reticulated platelets, we were able to distinguish platelets newly produced in IL-1α–treated mice from older conventionally produced platelets. The IL-1α–dependent platelets were larger in size than those in TPO-treated mice (Fig. 4, J and K), and anti-CD42b antibody increased the large platelet populations in control mice but not in IL-1R1$^{-/-}$ mice (Fig. S2). IL-1α–dependent platelets also had shorter lifetimes, which was not affected by clodronate-mediated macrophage suppression (Fig. 4 L), confirming the intrinsic nature of the lifetime. The particles released in vivo stained positively with mitochondrial membrane potential dyes, indicating intact mitochondrial function (Fig. S3 A). Platelets isolated from IL-1α–treated mice showed less JONA binding, but overall platelet aggregation in vitro and thrombus formation in vivo were comparable to the TPO-mediated responses. Thus, IL-1α stimulation leads to production of larger platelets with minor impairment but intact thrombotic function (Fig. S3).

IL-1α-induces MK differentiation, maturation, and MK rupture-dependent platelet biogenesis with PPF inhibition in vitro

IL-1α–induced MK rupture thrombopoiesis was also observed in fetal liver MKs, which enabled us to examine its molecular mechanism and to clarify differences from FasL-induced apoptosis (Fig. 5, A–D). As mentioned, the particles released from IL-1α–treated MKs were larger than those induced by TPO (Fig. 5 E). IL-1α increased the ploidy and number of MKs (Fig. 5, F and G), as well as the release of platelet-sized CD41^{+}CD42b^{+} particles (Fig. 5 H), indicating positive effects of IL-1α on MK differentiation, maturation, and platelet biogenesis, i.e., IL-1α increased MK rupture thrombopoiesis.

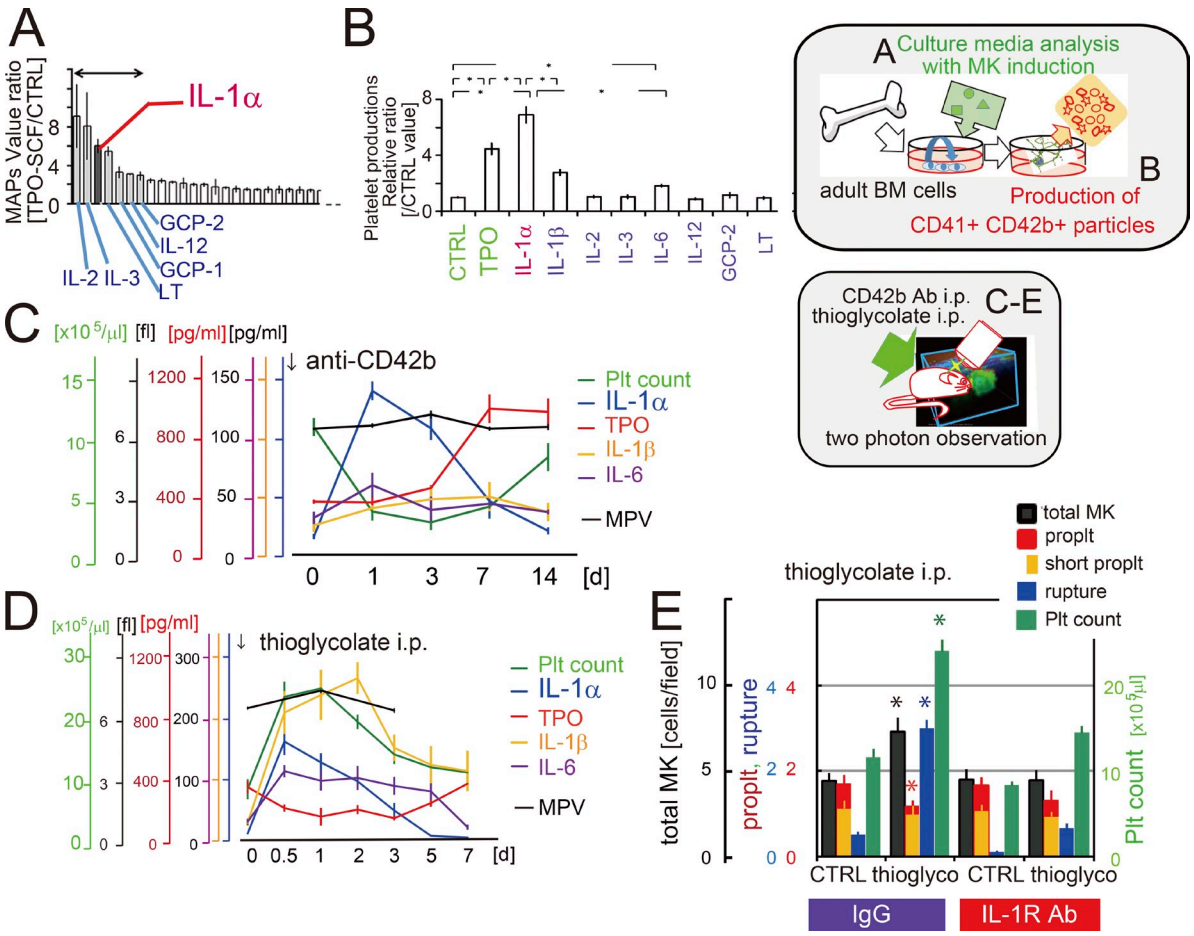

Figure 3. **IL-1α levels increase with acute platelet demands.** (A) Initial screening for thrombopoietic humoral factors in cultured BM cells. BM cells isolated from 6-wk-old WT mice were cultured without (CTRL) or with TPO (50 ng/ml) plus stem cell factor (SCF; 50 ng/ml). After culture for 7 d, secretion of humoral factors into the culture medium was assessed using MAPs analysis. Shown are the MAPs value ratios (TPO+SCF/CTRL). Seven factors with a ratio of >2.5 were identified. LT, lymphotactin; GCP, granulocyte chemotactic protein. *n* = 5 experiments. (B) BM cells were collected and then cultured in the presence of IL-1α, IL-1β, IL-2, IL-3, IL-6, LT, IL-12 subunit p70, or GCP-2. Production of $CD41^{+}CD42b^{+}$ particles was evaluated in the culture media after 7-d culture. The percent value was normalized to that of medium from vehicle-treated cells. *n* = 5 experiments. (C and D) Platelet counts, MPV values, and serum IL-1α, IL-1β, IL-6, and TPO levels after administration of anti-CD42b antibody (R300) (C) or thioglycolate (D). *n* = 5–8 animals in each group. (E) MK dynamics and platelet counts after thioglycolate-induced peritoneal inflammation in 6-wk-old CAG-eGFP mice, which were simultaneously treated with IgG or neutralizing anti–IL-1R antibody (100 µg/mouse.). *n* = 8 animals in each group. *, P < 0.05 versus CTRL group.

IL-1α stimulation induces caspase-3 activation without evident apoptosis

RT-PCR analysis of cultured fetal liver MKs showed that IL-1α increased expression of *Gata1*, *Bak1*, and *Bax*, which are known to be involved in thrombopoiesis and preapoptotic gene activation (Fig. 6 A; Kaushansky, 2003). Although there has been controversy regarding the caspase cascade in thrombopoiesis (De Botton et al., 2002; Clarke et al., 2003; Josefsson et al., 2014), IL-1α induced caspase-3 as well as p53 activation and AKT/ERK phosphorylation via IL-1R1 (Fig. 6, B–D; and Fig. S4). siRNA-mediated knockdown of IL-1R1 efficiently suppressed the pAKT–pERK signal (Fig. 6 C and Fig. S4), but *Thpo* and *Il1r1* expression in fetal liver MKs and TPO-R expression in isolated platelets were unaltered by IL-1α (Fig. 6, E and F). Immunofluorescence experiments also revealed the activation of caspase-3 and release of von Willebrand factor–positive granules, but TUNEL staining was negative, which makes this process different from typical FasL-induced apoptosis (Fig. 6, G–J). Caspase inhibition using Z-VAD (OMe)-FMK suppressed the effect of IL-1α on platelet counts in vivo (Fig. 6 K) and platelet-like particle releases in vitro (Fig. 5 H). Indeed, IL-1α–induced MK rupture thrombopoiesis was blocked in *Casp-3*$^{-/-}$ mice but not *Thpo*$^{-/-}$ mice (Fig. 6 L). These results indicate the rupture machinery is associated with caspase-3 activation via IL-1α/IL-1R1 but is distinct from TPO-dependent signaling and typical apoptosis.

IL-1α–treated MKs show impairment of proportional microtubule assembly

We next asked how IL-1α–IL-1R1 signaling with preapoptotic gene activation changes the mode of platelet generation from PPF to rupture (Fig. 7). It was previously shown that PPF-mediated platelet generation is microtubule dependent (Patel et al., 2005; Thon and Italiano, 2010; Kunishima et al., 2014; Machlus et al., 2014). To determine whether IL-1α influences microtubule dependency, two microtubule inhibitors (colchicine or paclitaxel), were administered to mice or fetal liver MKs with or without subsequent IL-1α treatment, after

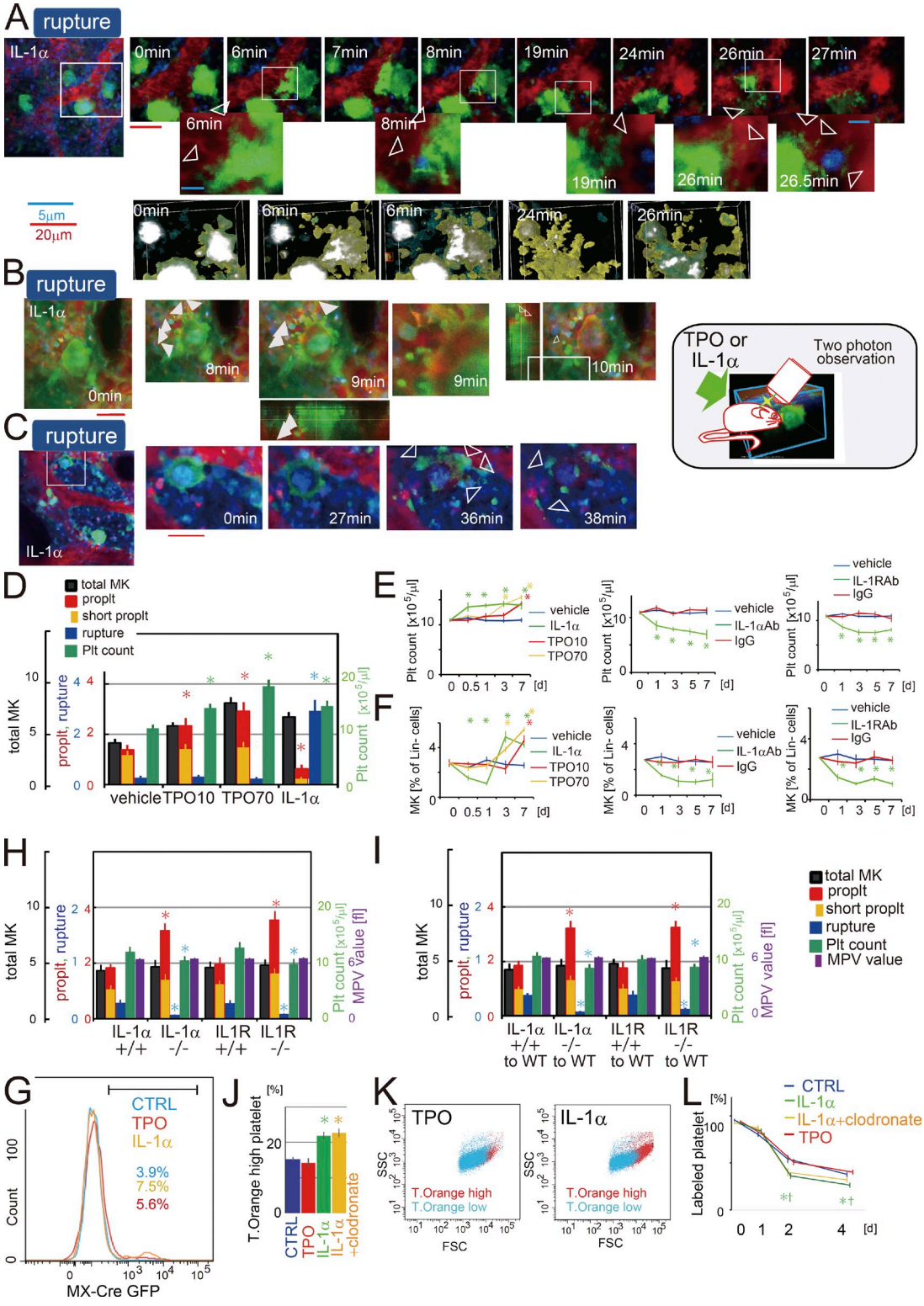

Figure 4. **IL-1α-induced MK rupture yields larger platelets.** (A–C) Time-lapse images of thrombopoiesis in living BM from 6-wk-old CAG-eGFP mice treated with IL-1α (10 µg/mouse s.c. daily for 5 d). (A, Video 8; B, Video 9; and C, Video 10.) (D) Quantification of MK dynamics and numbers and platelet counts in 6-wk-old CAG eGFP mice treated with TPO (10 µg/mouse s.c. daily for 5 d [TPO10], or with 70 µg/mouse daily for 3 d [TPO70]) or IL-1α (10 µg/mouse s.c. daily for 5 d). The BM was visualized and platelet counts were analyzed 7 d after the first administration. $n = 50$ high-power fields from 5 animals for each group. *, $P < 0.05$ versus vehicle treated mice. (E and F) Platelet counts in isolated blood (E) and the $CD41^+CD42b^+$ MK fraction among Lin^- BM cells (F) treated with vehicle (CTRL), low-, or high-dose TPO, IL-1α, anti–IL-1α neutralizing antibody (IL-1Ab), anti–IL-1R neutralizing antibody (IL-1RAb), or isotype-matched control antibody (IgG1 for IL-1Ab, IgG2 for IL-1RAb). All antibodies were used at 100 µg/mouse administered i.p. daily for 3 d. $n = 8$ animals in each group. (G) Identification of newly produced MKs using MX-Cre-GFP mice. GFP-labeled cells were analyzed among $Lin^-CD41^+CD42b^+$ BM cells 2 d after PIPC injection. The data shown are from a single representative experiment from among three repeats. (H) Quantification of thrombopoiesis under physiological conditions in 6-wk-old IL-1$\alpha^{+/+}$, IL-1 $\alpha^{-/-}$, IL-R1$^{+/+}$, and IL-1R1$^{-/-}$ mice. (I) MK dynamics in chimeric mice. $n = 50$ high-power fields from

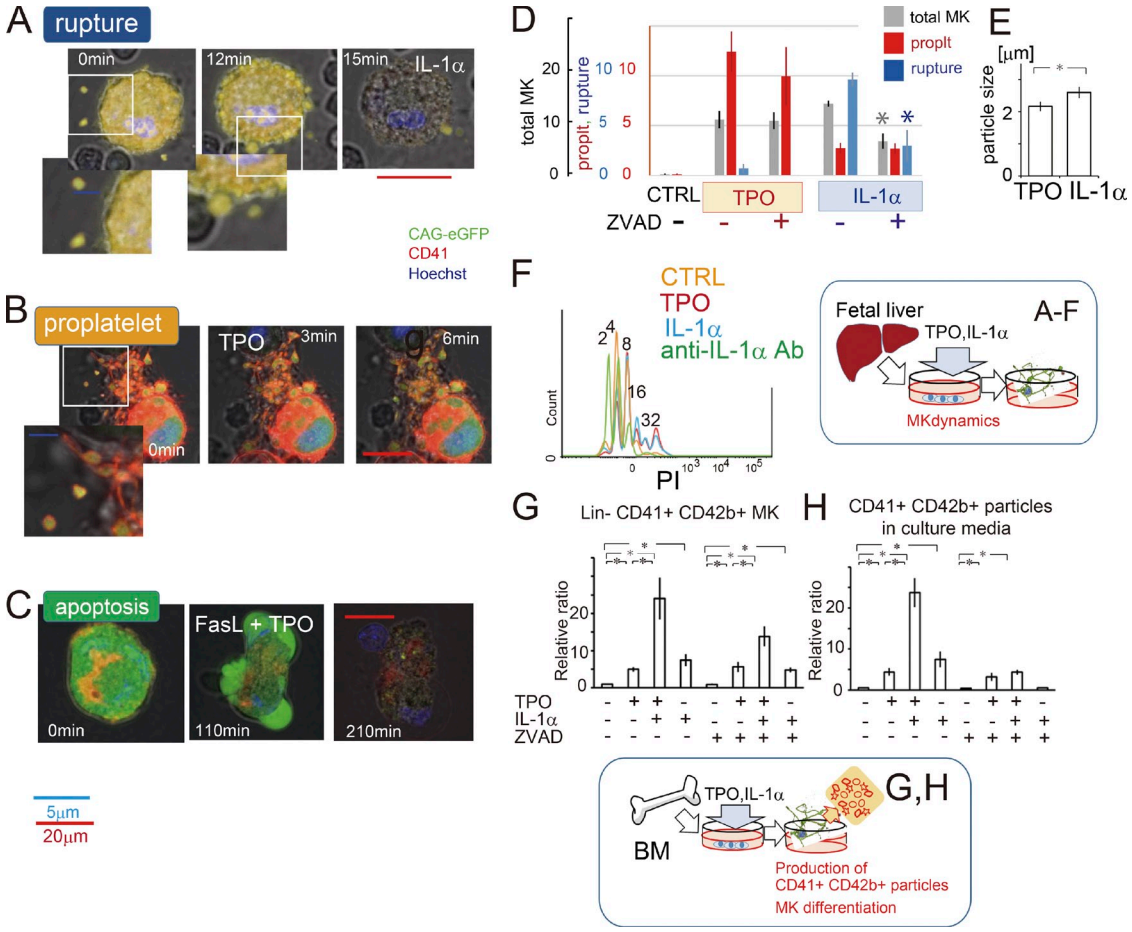

Figure 5. **IL-1α–induced MK differentiation and rupture-dependent platelet biogenesis in vitro.** (A–C) Time-lapse images of cultured MKs. Liver cells were collected from fetal CAG-eGFP mice on embryonic day 13 and cultured with TPO. On day 7 of culture, the cells were washed and incubated with anti-CD41 and Hoechst 33342. MKs were identified in the cultures as multinucleate and staining positive for CD41. MKs were then treated with TPO, IL-1α, or TPO plus Fas ligand 1 h before the experiments. Proplatelet production was observed in the presence of TPO, whereas MK rupture was seen in the presence of IL-1α. (D and E) Quantification of MK dynamics (D) and released particle size (E). *n* = 20 low-power fields (D) and *n* = 20 particles (E). Some cells were cultured with Z-VAD (OMe)-FMK (100 μM) 1 d before the experiments. (F) Fetal liver cells were isolated and cultured with TPO for 6 d. Differentiated MKs were washed and then incubated for 1 d with TPO, IL-1α, and anti–IL-1α neutralizing antibody. Ploidy was analyzed in $CD41^+CD42b^+Lin^-$ MKs. The data shown are from a single representative experiment from among three repeats. (G and H) BM cells isolated from 6-wk-old WT mice were cultured, and $CD41^+CD42b^+Lin^-$ MKs were counted (G) in each well after 7 d. The percent value was normalized to that of a control well. *n* = 5 experiments. (H) Release of $CD41^+CD42b^+$ particles into the culture medium. *n* = 5 experiments. *, $P < 0.05$.

which we examined whether the dynamics of platelet-like particle formation and release were suppressed by either drug in the presence of IL-1α (Fig. 7, A and B). Examination of tubulin immunofluorescence in fetal liver–derived MKs showed that IL-1α promoted formation of small vesicles in the periphery of MKs that all stained positive for β1-tubulin, but some were negative for α-tubulin (Fig. 7, C and D). However, TPO accelerated PPF, with the well-coordinated distribution of α- and β1-tubulin within MKs. TPO also similarly increased expression of both *Tuba1a* and *Tubb1*. In contrast, IL-1α induced a 10-fold increase in *Tubb1* expression, and a 50-fold increase when combined with TPO, while having no effect on *Tuba1a*, *Tuba1c*, or *Tuba4a* expression (Fig. 7 E and not depicted). We found the formation of a demarcation membrane system and development of platelet territories in IL-1α–treated MKs before membrane rupture (Fig. 7 F and Fig. S5). Platelets from $Thpo^{-/-}$ mice treated with IL-1α showed an absence of proper tubulin distribution, suggesting β1-tubulin oversupply, and those from IL-1α–treated WT mice are mostly spheroid shape rather than elongated shape by WT or TPO-treated platelets (Fig. 7, G–I; and Fig. S5). We concluded that IL-1α–induced disorganization of microtubule assembly accounts for the dysregulated α- and β1-tubulin synthesis, which should contribute to the PPF inhibition and MK rupture as a result.

5 animals in each group. *, $P < 0.05$ versus control mice. (J) Fractions of thiazole $orange^{high}$ platelets in isolated blood from WT mice treated with vehicle, TPO, IL-1α and/or clodronate. *n* = 5 mice. (K) Flow cytometric size analysis of thiazole $orange^{high}$ and thiazole $orange^{low}$ platelets in WT mice treated with TPO or IL-1α. (L) Platelet lifetimes in WT mice treated with vehicle, low-dose TPO, IL-1α, and/or clodronate. Platelets were labeled in vivo with anti-CD42c antibody (X488). During the gradual disappearance of circulating $X488^+$ platelets, we were able to distinguish newly generated platelets from previously circulating ones based on their X488 negativity. *n* = 5 mice. Bars, (red) 20 μm. *, $P < 0.05$.

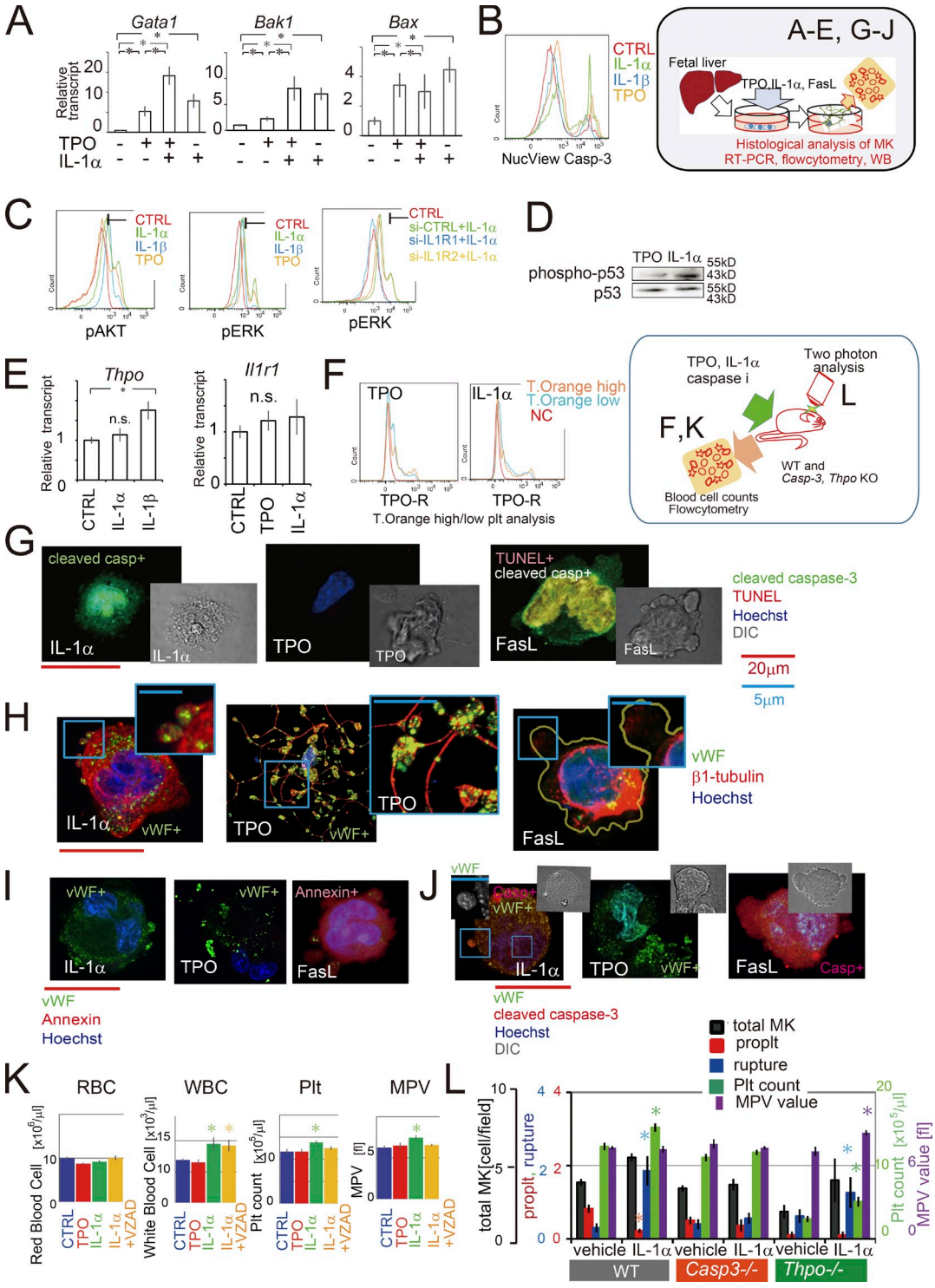

Figure 6. **IL-1α–induced atypical apoptosis with caspase-3 activation in fetal liver MKs.** (A and B) Liver cells were obtained from fetal WT mice on embryonic day 13, cultured with TPO or IL-1α, and analyzed on day 7. (A) RT-PCR analysis of gene expression in the harvested cells. The values were normalized to a vehicle-treated control. *n* = 5 experiments. (B) Flow cytometric analysis of caspase-3 activation in Lin$^-$CD41$^+$CD42b$^+$ MKs. (C) Fetal liver cells were cultured with TPO. siRNA-mediated knockdown was performed on day 4. On day 7, cells were washed, incubated with TPO, IL-1α, or IL-1β for an additional 1 d, and pAKT–pERK signaling in Lin$^-$CD41$^+$CD42b$^+$ MKs was analyzed on day 8. The data shown are from a single representative experiment from among three repeats (B and C). (D) Western blotting of p53 and phospho-p53 in fetal liver cells cultured with TPO and IL-1α from day 0 to 7. MKs were enriched with discontinuous albumin density gradient centrifugation. (E) Fetal liver cells were differentiated using TPO for 7 d, and then stimulated with vehicle, TPO, IL-1α, or IL-1β for an additional 1 d, after which gene expression was analyzed using RT-PCR. (F) Flow cytometric analysis of T. orange^{high} and T. orange^{low} platelets isolated from WT mice treated with TPO or IL-1α. NC denotes a negative control. The data shown are from a single representative experiment from among five repeats. (G–J) Immunofluorescence analysis of fetal liver MKs, which were cultured and differentiated from day 0 to 7 with TPO or IL-1α. Some cells were treated with Fas-ligand from day 6 to 7 after differentiation with TPO (FasL). Note that IL-1α–treated MKs were caspase-3–positive with release of von Willebrand factor–positive granules, but TUNEL staining was negative, which was different than typical FasL-induced apoptosis with blebbing. (K) Blood cell counts in WT mice treated with TPO, IL-1α, and/or Z-VAD (OMe)-FMK. (L) MK dynamics and platelet counts in WT, *Casp3*$^{-/-}$, and *Thpo*$^{-/-}$ mice treated with vehicle or IL-1α. *n* = 3–8 mice. Bars, (red) 20 μm. *, P < 0.05 versus CTRL group.

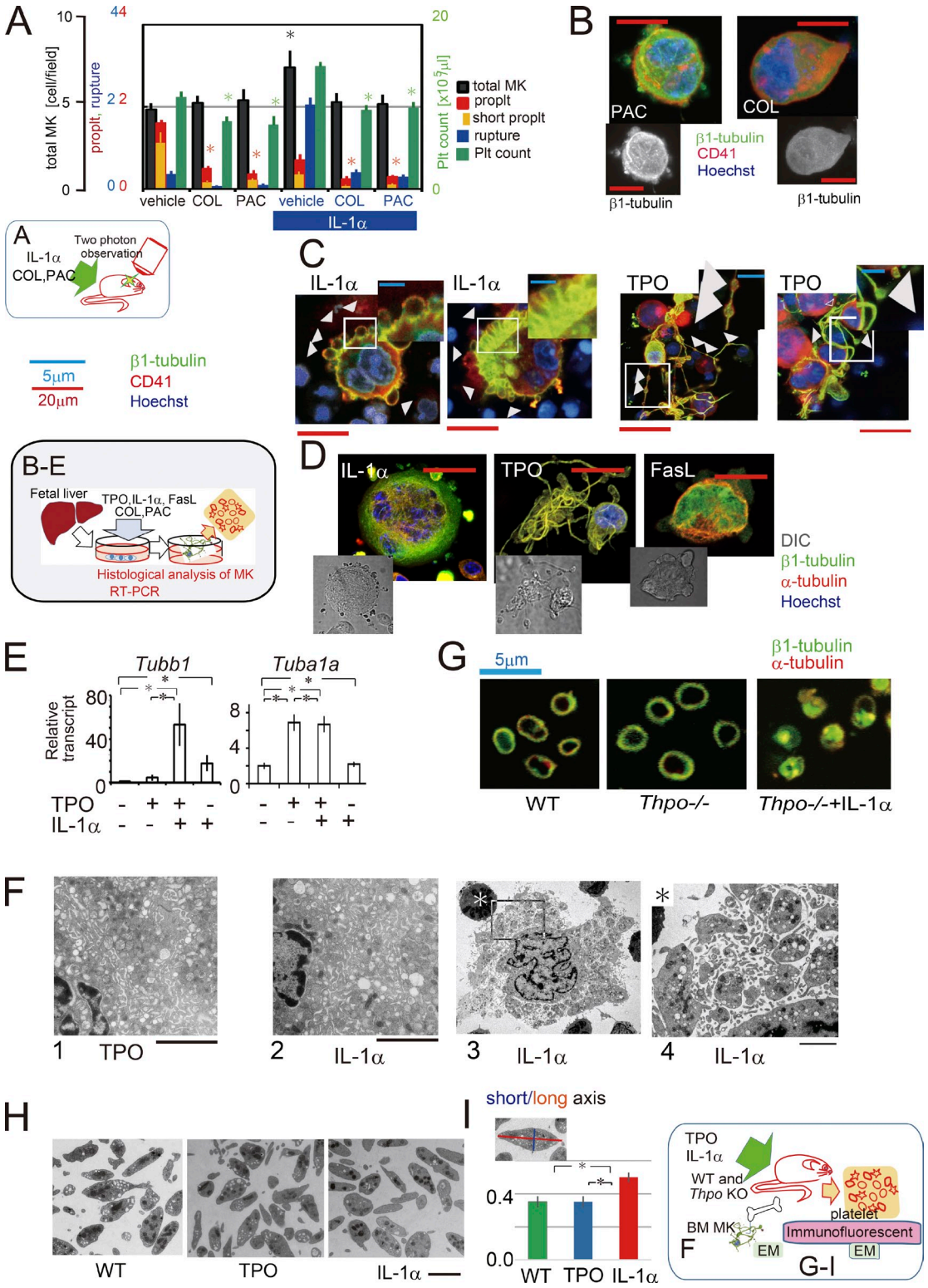

Figure 7. **IL-1α inhibited regulated tubulin assembly and proplatelet formation.** (A) Quantification of MK numbers and dynamics and platelet counts in 6-wk-old CAG-eGFP mice treated with IL-1α (10 μg for 5 d), colchicine (5 mg/kg i.v. once 6 h before experiments), and/or paclitaxel (10 mg/kg i.v. once 6 h before experiments). The BM was visualized and platelet counts were analyzed 7 d after the first administration. n = 24 high-power fields from 8 animals in each group. *, $P < 0.05$ versus control (WT) (B–D) Immunofluorescence analysis of fetal liver MKs cultured and differentiated from day 0 to 7 with TPO or IL-1α. In addition, the cells were treated with colchicine (2.5 μM) or paclitaxel (2.5 μM) from day 6 to day 7 (B). Some cells were also treated with Fas-ligand with TPO from day 6 to 7 (FasL). On day 7, the cells were fixed and stained (C and D). (E) RT-PCR analysis of gene expression in harvested cells. The values were normalized to vehicle-treated control. n = 8 experiments. (F) Electron microscopy of isolated BM MKs from TPO or IL-1α mice. Note that demarcation membrane system was similarly developed in two mice (1 and 2), before rupture, and fragments indicated several platelets (3 and 4). Bars, 2 μm. (G) Immunofluorescence study of tubulin distribution in platelets from WT, *Thpo*$^{-/-}$ mice, or *Thpo*$^{-/-}$ mice treated with IL-1α. (H) Electron microscopy of isolated platelets from WT mice treated with vehicle (WT), TPO, or IL-1α. (I) The short and long axis length was measured in randomly selected individual platelets, and ratio (short/long) was evaluated in 40 cells for each groups. Bars, 2 μm. *, $P < 0.05$.

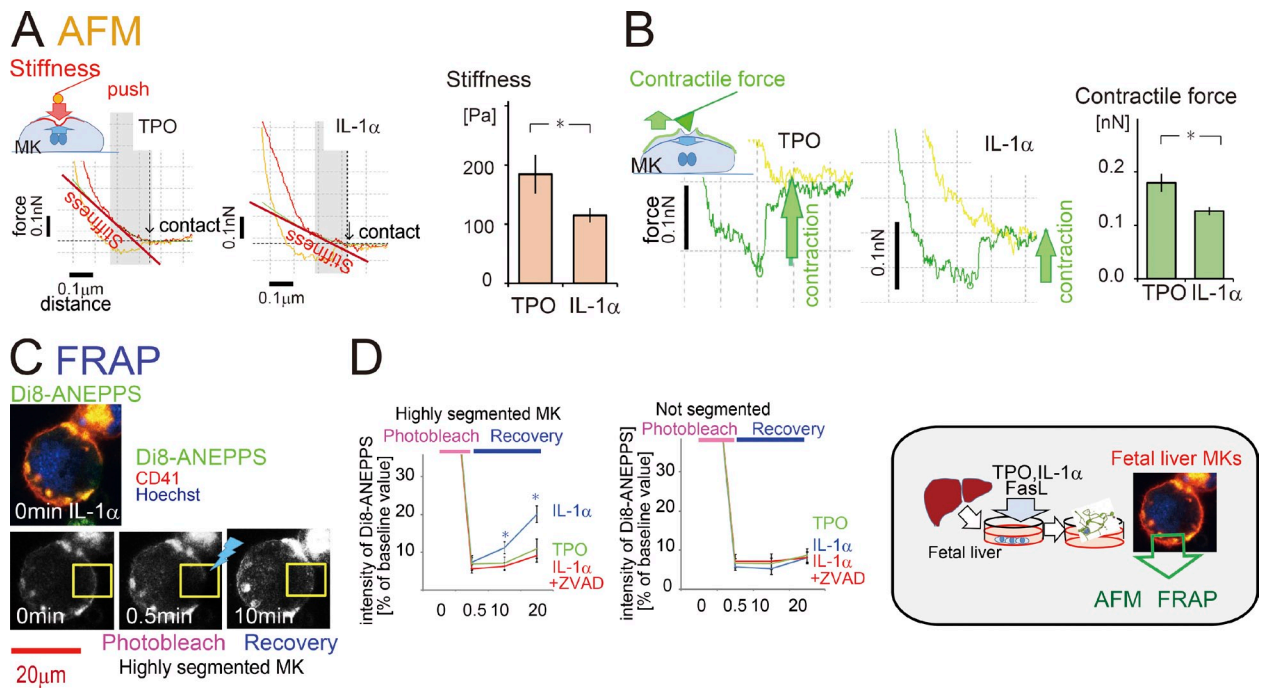

Figure 8. **IL-1α drives MK rupture thrombopoiesis by reducing functional and mechanical membrane stability in MKs.** (A and B) Fetal liver cells from WT mice were cultured for 7 d with IL-1α or TPO, after which MKs were evaluated using atomic force microscopy by pushing a bead-headed cantilever to measure stiffness (A) and pulling up on a membrane-attached cantilever to measure contractile force (B). Representative force-measurement curve, stiffness, and contractile force against cantilevers were shown. *n* = 20 measurements. (C and D) Fluorescence recovery after photobleaching (FRAP) analysis. Fetal liver MKs were cultured for 7 d with IL-1α or TPO. Some cells cultured with TPO were also treated with Z-VAD (OMe)-FMK (100 μM) 1 d before the experiments. MKs were stained with Di8-ANEPPS and then photobleached in a region of interest (ROI; red box). Restoration of Di8-ANEPPS intensity reflected membrane fluidity and instability. The left panels show representative snapshots during photobleaching and the corresponding Di8-ANEPPS signals. MKs were divided into mature highly segmented (more than two nuclear segmentations) and not segmented (one or two nuclear segmentations) groups. *n* = 20 examinations from 5 specimens. *, $P < 0.05$ versus TPO.

IL-1α induces mechanically and functionally weaker plasma membrane structure

The multiple functional changes seen in IL-1α–treated MKs before membrane rupture during thrombopoiesis were also examined. Using atomic force microscopy to evaluate MKs' ability to push a bead-attached cantilever or exert contractile force to pull up a cantilever, it was found that IL-1α–treated MKs were less stiff and thus exerted less force (Fig. 8, A and B). Fluorescent recovery after photobleaching (FRAP) analysis further confirmed that membrane stability was reduced in IL-1α–treated mature polyploid MKs, but not in mononuclear CD41$^+$ cells (immature MKs), and that it was restored by caspase inhibition (Z-VAD [OMe]-FMK; Fig. 8, C and D; Ahn et al., 2002). These results strongly indicate that IL-1α reduces plasma membrane potential, which leads to a mechanically and functionally weaker membrane structure and drives MKs toward MK rupture thrombopoiesis.

Discussion

Novel MK rupture thrombopoiesis

In vitro platelet biogenesis from fetal liver MKs, human CD34$^+$ cells, embryonic stem cells, or induced pluripotent stem cells all consistently show the presence of PPF and release of fragments from the tips of elongated pseudopodal structures under steady-state and TPO-stimulated conditions (Italiano et al., 1999; Eto et al., 2007; Takayama et al., 2010). However, although recent in vivo imaging-based analyses confirmed the presence of PPF (Junt et al., 2007; Zhang et al., 2012), we found that the number of platelets produced from each MK was both consistent with previously reported numbers (Thon et al., 2012; Avanzi and Mitchell, 2014) and too low for an adequate response to acute platelet needs or inflammatory stimuli.

Herein we demonstrated an alternative MK rupture–type thrombopoietic process, which can provide 20 times more platelets than PPF, released primarily into BM vessels within 1 h (Fig. 1 D), and which we visualized for the first time using high-speed two-photon microscopy with multicolor high-sensitive GaAs detectors (Fig. 1). The novel MK rupture–dependent pathway is primarily regulated by the inflammatory cytokine IL-1α, and is morphologically and mechanically distinct from PPF and typical FasL-induced apoptosis, as well as from the recently reported cytoplasmic elongation of large platelet progenitor structures (Thon and Italiano, 2010; Kowata et al., 2014), as summarized in Table S1 and Fig. 9.

Ng et al. (2014) recently reported that MK maturation and final platelet shedding can both be independent of TPO signaling, but they did not address alternatives to TPO. In this study, we found that IL-1α–IL1R1 signaling positively influences the MK differentiation phase, as well as platelet shedding through rupture, which compensated for the deficiency of TPO signaling in MKs (Ng et al., 2014). In addition, a shear-dependent

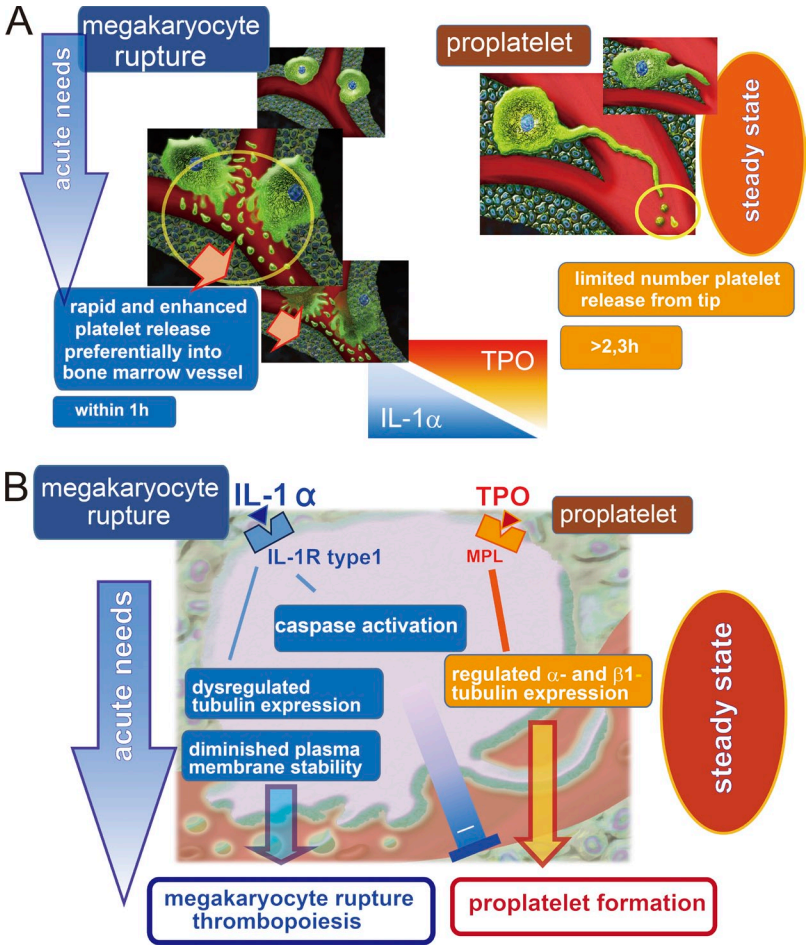

Figure 9. **Schematic model of the two modes of thrombopoiesis.** (A) Morphological features of BM MKs with proplatelet formation and MK rupture type thrombopoiesis. (B) Dysregulation of tubulin expression and instability of plasma membrane of MK with rupture.

mechanism may also promote TPO-independent platelet generation (Jiang et al., 2014).

MKs respond to acute platelet demand via IL-1α

Under acute inflammatory or cytopenic conditions, rapid elevation of IL-1α promoted a change in cell programing to MK rupture thrombopoiesis (Fig. 2 and 3). Reductions in platelet counts during acute inflammation induced by neutralizing anti–IL-1α antibody indicate that an urgent requirement for platelet recruitment or recovery as a host defense may be associated with inflammation-mediated elevation of IL-1α levels, as reported previously (Rider et al., 2011). However, serum levels of multiple inflammatory cytokines, including IL-1β, IL-2, IL-6, and IL-11, were also elevated and may contribute to the increase in platelet production (Fig. 3). Although IL-1β, produced from platelets during acute inflammation, reportedly stimulates MK polyploidization (Yang et al., 2000; Denis et al., 2005; Beaulieu et al., 2014), the levels of IL-1β were not associated with elevation of platelets after administration of anti-CD42b antibody (Fig. 3 C). This result is consistent with the fact that the phenotypes of IL-1α and IL-1β knockout mice differ from one another (Nambu et al., 2006).

IL-1α–treated MKs showed clear changes to their cell membrane before MK rupture (Fig. 8). The plasma membrane was functionally and mechanically less stable in IL-1α–treated MKs. Instability of membrane structure after IL-1α treatment may also be associated with platelet shape in generation. Platelets by IL-1α appeared to display more spheroid but PPF-dependent platelets were longitudinal (Fig. 7, G–I; and Fig. S5), as demonstrated previously (Thon and Italiano, 2010). Interestingly, this membrane instability was dependent on caspase activity in only mature MKs (Fig. 8 D). That the action of IL-1α in MK rupture thrombopoiesis was caspase-3 dependent (Fig. 6, K and L) suggests caspase activation may occur downstream of the IL-1α–ILR1 axis in association with alteration of the cell membrane structure. The caspase-dependent thrombopoiesis theory has been discussed for a long time (De Botton et al., 2002; Clarke et al., 2003; Josefsson et al., 2014). Our data provide evidence of caspase dependency in platelet biogenesis; however, the caspase involvement is independent of TPO-mediated PPF, as recently demonstrated (Josefsson et al., 2014). But the detailed mechanism of caspase activation or p53 up-regulation in MK rupture thrombopoiesis must be elucidated further.

In conclusion, our findings provide direct evidence that IL-1α is an acute platelet releasing factor that induces enhanced platelet release through rupture of the mature MK membrane. This novel mechanism may enable rapid restoration in platelet numbers, but with insufficient microtubule organization. It appears the balance between TPO and IL-1α determines the cellular programming of MKs for thrombopoiesis in response to acute and chronic platelet needs.

Materials and methods

Mice

WT C57BL/6J, B6 and B6.129S7-*Il1r1*^{tm1Imx}/J IL (IL-1R knockout) mice were obtained from Japan Charles River Laboratories. A null mutation in *Il1r1* was generated by homologous recombination using a replacement vector in which a 2.4-kb EcoR1–Pst1 fragment encompassing two exons was replaced with a PGKneo cassette. B6.Cg-*Tg(Mx1-cre)1Cgn/J* mice were gifts from the Institute of Physical and Chemical Research ([RIKEN] Saitama, Japan). The transgenes used were the mouse Mx1 gene promoter, nuclear localization sequence-modified Cre recombinase and a fragment from the human growth hormone gene. *B6.Cg-Tg(CAG-floxed Neo-EGFP)REP08Osb* mice carrying the transgene for the CAG promoter and EGFP cDNA separated by a floxed neo cassette were a gift from Riken (Matsumura et al., 2004). *IL-1*$\alpha^{-/-}$ mice were provided by Y. Iwakura (Tokyo University of Science, Tokyo, Japan; Horai et al., 1998). A null mutation in *IL-1*α was generated using a replacing vector in which a 1.5-kb DNA fragment between the Sau3AI and KpnI sites in exon 5 and intron 5, respectively, was replaced with a lacZ-pA-PGK-hph-pA cassette. B6N.129S1-*Casp3*^{tm1Flv}*/J (Casp-3*$^{-/-}$*)* mice were obtained from Japan Charles River Laboratories. A targeting vector was designed to replace the caspase protease-conserved catalytic site of the endogenous gene with a PGK-neo cassette. *Thpo* KO mice were generated using a targeting vector to remove exon 3 by inserting a neo cassette, and were provided by B. Heissig (The University of Tokyo, Tokyo, Japan; de Sauvage et al., 1996).

Animal models

To assess the contributions made by humoral factors, 5-wk-old CAG-eGFP mice were treated with TPO (Sigma-Aldrich) or IL-1α (R&D Systems or BioLegend) at dosages of 10 µg/mouse subcutaneously (SC) daily for 5 d or 70 µg/mouse SC daily for 3 d. The mice were visualized and examined at 6-wk-old, 7 d after the first treatment. Some mice were also treated with neutralizing antibodies against IL-1α (R&D Systems or BioLegend), IL-1R (BioLegend), isotype-matched control antibody (BioLegend), or Fas Ligand (5 µg/mouse i.v.; R&D Systems). All antibodies were administered at 100 µg/mouse i.p. daily for 3 d.

To assess the effect of acute inflammation, thioglycolate (Sigma-Aldrich) was administered i.p. (3 ml of 3% solution/mouse once). To examine the effect of caspase inhibition, mice were treated with the pan-caspase inhibitor Z-VAD (OMe)-FMK (3 mg/kg IP daily for 5 d; Merck Millipore). Clophosome (200 µl/mouse; FormuMax Scientific Inc.) was administered i.p. to deplete macrophages.

To obtain chimeric mice, 6-wk-old WT mice were lethally irradiated at a dose of 9.5 Gy, after which they were transplanted with BM total cells from age-matched IL-1R$^{-/-}$/CAG-eGFP, IL-1$\alpha^{-/-}$/CAG-eGFP, or control (IL-1R$^{+/+}$/CAG-eGFP or IL-1$\alpha^{+/+}$/CAG-eGFP) mice. 6 wk after transplantation, BM dynamics were scored.

Intravital microscopy for thrombopoiesis in living BM

To visualize MK dynamics in scalp BM, we used in vivo multiphoton microscopy, which is a modification of the single photon intravital visualization technique (Nishimura et al., 2008; Takizawa et al., 2010). CAG-eGFP and CD41-tdTomato mice were anesthetized by injection with urethane (1.5 g/kg), after which the scalp skin was removed, and the mice were secured to the heated piezo-drive stage (Tokai Hit; Nikon) of an inverted microscope (Eclipse Ti; Nikon). Texas Red-dextran (25 mg/kg BW) and Hoechst 33342 (10 mg/kg) were injected to visualize cell dynamics and blood flow. Use of this approach for identification was validated through flow cytometric analysis of samples of scalp and femur BM and direct intravital staining with an anti-CD41 antibody (Fig. S1). The tissue was excited at a wavelength of 920 nm using a Ti:sapphire laser (Vision II; Coherent), and images were captured as XYZ-T images using an A1R-MP system (Nikon); the X direction was scanned using a resonance mirror, the Y direction using a galvano mirror, and the Z direction using the piezo-drive stage. Because highly sensitive GaAs detectors were used, the laser power usually did not exceed 15% of the maximum for the Vision II laser. A 40× (N.A. 1.15) water immersion objective lens (Nikon) was used, and the images were captured at 1.5× zoom. The dwelling time for one pixel was 0.1 µs. Z-stacks were usually 60 µm thick and composed of ∼1-µm slice images. We also avoided phototoxicity by first characterizing the effects of the laser and reactive oxygen scavengers.

Image analysis

In each experiment involving intravital visualization, >10 high-power field XYZ-T images were acquired. The collected data were analyzed and visualized using an automatic algorithm in NIS-Elements (Nikon) and custom designed software (IMAGICA Imageworks). Slice, voxel, and maximum intensity projection views are provided in the figures and videos. Also calculated by the software were the particle release, time-dependent changes in MK perimeters, and the cytoplasmic GFP signal. After measuring the proplatelet long axis, a >50% increase in perimeter (deformity) and a decrease in the cytoplasmic GFP signal intensity (rupture) were identified as the rupture pattern. Alternatively, MKs showing long arm projections (>50% of the length of the average cell diameter) were deemed to contain proplatelets, and we categorized long (>100 µm) and short (<100 µm) proplatelet formation based on the arm length. The total numbers of rupture-type and proplatelet-type MKs detected during the observation periods were counted.

Fetal liver cell cultures

Liver cells were collected from fetal WT mice on embryonic day (E) 13. Single-cell suspensions, prepared through successive passaging, were cultured in DMEM supplemented with 10% FCS without (CTRL) or with TPO (50 ng/ml), SCF (50 ng/ml), Fas ligand (1 µg/ml), and/or IL-1α (50 ng/ml). On day 7 of culture, the cells were washed and analyzed. MKs were enriched by discontinuous albumin density gradient centrifugation before analysis. Caspase activation was evaluated using NucView Caspase-3 (Biotium; Bosch and Franklin-Tong, 2007). The mechanical properties of cultured fetal liver MKs were evaluated using atomic force microscopy (Nanowizard JPK Instruments AG) with bead-attached or sharp-head cantilevers.

For time-lapse imaging, some cells were washed and incubated with RPE-conjugated rat anti-CD41 (MWReg30) and Hoechst 33342. Differentiated MKs, identified as multinucleate and staining positively for CD41, were visualized at 37°C in DMEM using a confocal microscope (Nikon A1R) with a 100× (N.A. 1.25) oil immersion objective lens (Nikon).

FRAP analysis

To evaluate plasma membrane stability, we performed FRAP analysis with cultured fetal liver MKs. The MKs were stained with Di8-ANEPPS (5 µM), after which selected regions of interest (ROIs) were photobleached for 30 s. After photobleaching, Di8-ANPPES intensities within ROI lesions were continuously recorded using a single-photon confocal microscope (Nikon-A1R). The spontaneous recovery of the ROI signals was evaluated as an index of membrane stability/fragility, as previously reported (Ahn et al., 2002).

Immunofluorescence study

For immunofluorescence analyses, the cells were fixed in 4% paraformaldehyde for 45 min and permeabilized with 1% Triton X-100 (EMD Millipore) for 10 min. Thereafter, the specimens were blocked and incubated first for 12 h with a primary antibody (rabbit anti–β1-tubulin [Patel-Hett et al., 2008], rat anti-CD41 [MWReg30; BioLegend], rabbit anti-von Willebrand factor [Emfret], or rabbit anti-active caspase-3 [Millipore]. They were then incubated for 1 h with an RPE-conjugated rat anti-CD41 (MWReg30), Alexa Fluor–conjugated mouse anti–α-tubulin (Invitrogen) and/or goat secondary antibody (Invitrogen). Finally, the cells were counterstained for 1 h with Hoechst 33342, and images were captured using a confocal microscope (Nikon A1R). The cells were excited using three laser lines (405 nm, 488 nm, and 561 nm), and the emission was collected using appropriate narrow band-pass filters and GaAs detectors.

Electron microscopy

For electron microscopy, MKs were fixed in a mixture of 0.5% glutaraldehyde and 2% paraformaldehyde, washed, and post-fixed with 1% osmium tetroxide. After dehydration, the collected pellets were embedded in Epoxy resin. Ultrathin sections (60–80 nm thick) were then cut and stained with 2% uranyl acetate and Reynolds' lead citrate. Samples were observed in a transmission electron microscope (HT7700; Hitachi) operating at 80 kV.

Preparation of cells and flow cytometry

As previously described (Nishimura et al., 2009), we isolated BM cells from the scalp and femurs by flushing them with PBS, and collected blood samples from tail veins or by cardiac puncture under anesthesia. The cells were washed twice with PBS, incubated for 8.5 min in erythrocyte-lysing buffer, and finally suspended in PBS supplemented with 3% fetal bovine serum. The isolated cells were then incubated with FcBlock antibody (BD) for 15 min on ice, labeled with dye-conjugated antibodies, and analyzed by flow cytometry using a Canto II flow cytometer (BD), spectrum analyzer SP6800 (Sony), and FlowJo 7.2.2. software (Tomy Digital Biology). Propidium iodide (Invitrogen) or a Zombie NIR kit (BioLegend) was used to exclude dead cells. Conventional approaches, including Western blotting,

cannot be applied to assess intracellular signals in MKs isolated from mice due to the small sample size. We therefore used flow cytometry for signal analysis.

Flow cytometry–based platelet aggregation assays were also performed using previously reported methods with some modification (De Cuyper et al., 2013). Platelet-rich plasma and whole blood were obtained and incubated with RPE-conjugated anti-CD41 (MWReg30; BioLegend) or FITC-conjugated anti-CD61 (Luc.H11; Emfret) antibody, after which the two populations of labeled cells were mixed, 1:1, and incubated at 37°C. The cells were then activated with thrombin (Sigma-Aldrich; 5 U/ml), fixed in 0.5% formaldehyde at the indicated times thereafter, and analyzed using a Canto II flow cytometer (BD). The appearance of two-color events was considered to reflect aggregated platelets.

Western blotting

Western blotting was conducted with fetal liver cells enriched through discontinuous albumin density gradient centrifugation using rabbit anti-p53 (Santa Cruz Biotechnology, Inc.), or rabbit anti–phospho-p53 (Ser15; Cell Signaling Technology) antibodies.

Real-time quantitative PCR

For real-time PCR, total RNA was isolated using TRIzol (Invitrogen) and relative mRNA levels were determined using a Superarray kit (Superarray).

Statistics

Statistical analysis was performed using JMP (SAS) and Excel 2013 (Microsoft) software. Results were expressed as means ± SEM. The statistical significance of differences between two groups was evaluated using Student's *t* tests. Differences between more than two groups were evaluated using ANOVA followed by post-hoc Bonferroni tests. Correlations were evaluated using the Pearson correlation coefficient test. Values of $P < 0.05$ were considered significant.

Online supplemental material

Fig. S1 shows intravital visualization and validation study of BM MKs. Fig. S2 shows MK phenotype of IL-1 $\alpha^{-/-}$ and IL-1R1$^{-/-}$ mice, and serum TPO levels after IL-1 α treatment. Fig. S3 shows thrombus formation function of IL-1α–induced platelets. Fig. S4 shows intracellular signal analysis of IL-1α–treated MKs. Fig. S5 shows electron microscopic analysis of TPO- and IL-1α–induced platelets. Online supplemental material is available at http://www.jcb.org/cgi/content/full/jcb.201410052/DC1.

We are very grateful to M. Taniguchi, C. Yoshinaga, M. Tajima, X. Yingda, and T. Hirabayashi for their excellent technical help. We appreciate the gifts of mice from Drs. Heissig and Iwakura.

This study was supported by the Funding Program for Next Generation World-Leading Researchers (S. Nishimura); the Funding Program for World-Leading Innovative R&D on Science and Technology (FIRST Program; R. Nagai); the Translational Systems Biology, Medicine Initiative (S. Nishimura and T. Kadowaki), and PRESTO (S. Nishimura) from the Japan Science and Technology Agency (JST), the Project of Realization of Regenerative Medicine and Highway from MEXT/JST (K. Eto); and the Initiative for Accelerating Regulatory Science in Innovative Drug, Medical Device, and Regenerative Medicine from the Ministry of Health, Labor and Welfare (K. Eto).

S. Nishimura and K. Eto have applied for a patent related to this manuscript. K. Eto is a founder of Megakaryon Co. Ltd. J.E. Italiano Jr. has a financial interest in and is a founder of Platelet BioGenesis. The interests of J.E. Italiano Jr. were reviewed and are managed by the Brigham and Women's Hospital and Partners HealthCare in accordance with their conflict-of-interest policies. The other authors have no additional financial interests.

Author contributions: S. Nishimura, J.E. Italiano Jr., and K. Eto designed and performed experiments and worked on the manuscript. M. Nagasaki, A. Sawaguchi, T. Ohmori, A. Sakata, H. Sakaguchi, and T. Ryu performed experiments. I. Komuro and N. Takayama supervised research. S. Kunishima supervised research and worked on the manuscript. I. Komuro, T. Kadowaki, and R. Nagai designed experiments and worked on the manuscript.

Submitted: 15 October 2014
Accepted: 8 April 2015

References

Ahn, H.J., I.P. Sohn, H.C. Kwon, D.H. Jo, Y.D. Park, and C.K. Min. 2002. Characteristics of the cell membrane fluidity, actin fibers, and mitochondrial dysfunctions of frozen-thawed two-cell mouse embryos. *Mol. Reprod. Dev.* 61:466–476. http://dx.doi.org/10.1002/mrd.10040

Avanzi, M.P., and W.B. Mitchell. 2014. Ex vivo production of platelets from stem cells. *Br. J. Haematol.* 165:237–247. http://dx.doi.org/10.1111/bjh.12764

Beaulieu, L.M., E. Lin, E. Mick, M. Koupenova, E.O. Weinberg, C.D. Kramer, C.A. Genco, K. Tanriverdi, M.G. Larson, E.J. Benjamin, and J.E. Freedman. 2014. Interleukin 1 receptor 1 and interleukin 1β regulate megakaryocyte maturation, platelet activation, and transcript profile during inflammation in mice and humans. *Arterioscler. Thromb. Vasc. Biol.* 34:552–564. http://dx.doi.org/10.1161/ATVBAHA.113.302700

Bosch, M., and V.E. Franklin-Tong. 2007. Temporal and spatial activation of caspase-like enzymes induced by self-incompatibility in Papaver pollen. *Proc. Natl. Acad. Sci. USA*. 104:18327–18332. http://dx.doi.org/10.1073/pnas.0705826104

Clarke, M.C., J. Savill, D.B. Jones, B.S. Noble, and S.B. Brown. 2003. Compartmentalized megakaryocyte death generates functional platelets committed to caspase-independent death. *J. Cell Biol.* 160:577–587. http://dx.doi.org/10.1083/jcb.200210111

De Botton, S., S. Sabri, E. Daugas, Y. Zermati, J.E. Guidotti, O. Hermine, G. Kroemer, W. Vainchenker, and N. Debili. 2002. Platelet formation is the consequence of caspase activation within megakaryocytes. *Blood*. 100:1310–1317. http://dx.doi.org/10.1182/blood-2002-03-0686

De Cuyper, I.M., M. Meinders, E. van de Vijver, D. de Korte, L. Porcelijn, M. de Haas, J.A. Eble, K. Seeger, S. Rutella, D. Pagliara, et al. 2013. A novel flow cytometry-based platelet aggregation assay. *Blood*. 121:e70–e80. http://dx.doi.org/10.1182/blood-2012-06-437723

de Sauvage, F.J., P.E. Hass, S.D. Spencer, B.E. Malloy, A.L. Gurney, S.A. Spencer, W.C. Darbonne, W.J. Henzel, S.C. Wong, W.J. Kuang, et al. 1994. Stimulation of megakaryocytopoiesis and thrombopoiesis by the c-Mpl ligand. *Nature*. 369:533–538. http://dx.doi.org/10.1038/369533a0

de Sauvage, F.J., K. Carver-Moore, S.M. Luoh, A. Ryan, M. Dowd, D.L. Eaton, and M.W. Moore. 1996. Physiological regulation of early and late stages of megakaryocytopoiesis by thrombopoietin. *J. Exp. Med.* 183:651–656. http://dx.doi.org/10.1084/jem.183.2.651

Denis, M.M., N.D. Tolley, M. Bunting, H. Schwertz, H. Jiang, S. Lindemann, C.C. Yost, F.J. Rubner, K.H. Albertine, K.J. Swoboda, et al. 2005. Escaping the nuclear confines: signal-dependent pre-mRNA splicing in anucleate platelets. *Cell*. 122:379–391. http://dx.doi.org/10.1016/j.cell.2005.06.015

Eto, K., H. Nishikii, T. Ogaeri, S. Suetsugu, A. Kamiya, T. Kobayashi, D. Yamazaki, A. Oda, T. Takenawa, and H. Nakauchi. 2007. The WAVE2/Abi1 complex differentially regulates megakaryocyte development and spreading: implications for platelet biogenesis and spreading machinery. *Blood*. 110:3637–3647. http://dx.doi.org/10.1182/blood-2007-04-085860

Horai, R., M. Asano, K. Sudo, H. Kanuka, M. Suzuki, M. Nishihara, M. Takahashi, and Y. Iwakura. 1998. Production of mice deficient in genes for interleukin (IL)-1α, IL-1β, IL-1α/β, and IL-1 receptor antagonist shows that IL-1β is crucial in turpentine-induced fever development and glucocorticoid secretion. *J. Exp. Med.* 187:1463–1475. http://dx.doi.org/10.1084/jem.187.9.1463

Italiano, J.E., Jr., P. Lecine, R.A. Shivdasani, and J.H. Hartwig. 1999. Blood platelets are assembled principally at the ends of proplatelet processes produced by differentiated megakaryocytes. *J. Cell Biol.* 147:1299–1312. http://dx.doi.org/10.1083/jcb.147.6.1299

Jiang, J., D.S. Woulfe, and E.T. Papoutsakis. 2014. Shear enhances thrombopoiesis and formation of microparticles that induce megakaryocytic differentiation of stem cells. *Blood*. 124:2094–2103. http://dx.doi.org/10.1182/blood-2014-01-547927

Josefsson, E.C., D.L. Burnett, M. Lebois, M.A. Debrincat, M.J. White, K.J. Henley, R.M. Lane, D. Moujalled, S.P. Preston, L.A. O'Reilly, et al. 2014. Platelet production proceeds independently of the intrinsic and extrinsic apoptosis pathways. *Nat. Commun.* 5:3455. http://dx.doi.org/10.1038/ncomms4455

Junt, T., H. Schulze, Z. Chen, S. Massberg, T. Goerge, A. Krueger, D.D. Wagner, T. Graf, J.E. Italiano Jr., R.A. Shivdasani, and U.H. von Andrian. 2007. Dynamic visualization of thrombopoiesis within bone marrow. *Science*. 317:1767–1770. http://dx.doi.org/10.1126/science.1146304

Kaushansky, K. 2003. Thrombopoietin: a tool for understanding thrombopoiesis. *J. Thromb. Haemost.* 1:1587–1592. http://dx.doi.org/10.1046/j.1538-7836.2003.00273.x

Kowata, S., S. Isogai, K. Murai, S. Ito, K. Tohyama, M. Ema, J. Hitomi, and Y. Ishida. 2014. Platelet demand modulates the type of intravascular protrusion of megakaryocytes in bone marrow. *Thromb. Haemost.* 112:743–756. http://dx.doi.org/10.1160/TH14-02-0123

Kunishima, S., S. Nishimura, H. Suzuki, M. Imaizumi, and H. Saito. 2014. TUBB1 mutation disrupting microtubule assembly impairs proplatelet

formation and results in congenital macrothrombocytopenia. *Eur. J. Haematol.* 92:276–282. http://dx.doi.org/10.1111/ejh.12252

Kuter, D.J. 2007. New thrombopoietic growth factors. *Blood*. 109:4607–4616. http://dx.doi.org/10.1182/blood-2006-10-019315

Machlus, K.R., J.N. Thon, and J.E. Italiano Jr. 2014. Interpreting the developmental dance of the megakaryocyte: a review of the cellular and molecular processes mediating platelet formation. *Br. J. Haematol.* 165:227–236. http://dx.doi.org/10.1111/bjh.12758

Matsumura, H., H. Hasuwa, N. Inoue, M. Ikawa, and M. Okabe. 2004. Lineage-specific cell disruption in living mice by Cre-mediated expression of diphtheria toxin A chain. *Biochem. Biophys. Res. Commun.* 321:275–279. http://dx.doi.org/10.1016/j.bbrc.2004.06.139

Nakamura-Ishizu, A., K. Takubo, M. Fujioka, and T. Suda. 2014. Megakaryocytes are essential for HSC quiescence through the production of thrombopoietin. *Biochem. Biophys. Res. Commun.* 454:353–357. http://dx.doi.org/10.1016/j.bbrc.2014.10.095

Nambu, A., S. Nakae, and Y. Iwakura. 2006. IL-1beta, but not IL-1alpha, is required for antigen-specific T cell activation and the induction of local inflammation in the delayed-type hypersensitivity responses. *Int. Immunol.* 18:701–712. http://dx.doi.org/10.1093/intimm/dxl007

Ng, A.P., M. Kauppi, D. Metcalf, C.D. Hyland, E.C. Josefsson, M. Lebois, J.G. Zhang, T.M. Baldwin, L. Di Rago, D.J. Hilton, and W.S. Alexander. 2014. Mpl expression on megakaryocytes and platelets is dispensable for thrombopoiesis but essential to prevent myeloproliferation. *Proc. Natl. Acad. Sci. USA*. 111:5884–5889. http://dx.doi.org/10.1073/pnas.1404354111

Nishimura, S., I. Manabe, M. Nagasaki, K. Seo, H. Yamashita, Y. Hosoya, M. Ohsugi, K. Tobe, T. Kadowaki, R. Nagai, and S. Sugiura. 2008. In vivo imaging in mice reveals local cell dynamics and inflammation in obese adipose tissue. *J. Clin. Invest.* 118:710–721.

Nishimura, S., I. Manabe, M. Nagasaki, K. Eto, H. Yamashita, M. Ohsugi, M. Otsu, K. Hara, K. Ueki, S. Sugiura, et al. 2009. CD8+ effector T cells contribute to macrophage recruitment and adipose tissue inflammation in obesity. *Nat. Med.* 15:914–920. http://dx.doi.org/10.1038/nm.1964

Patel, S.R., J.H. Hartwig, and J.E. Italiano Jr. 2005. The biogenesis of platelets from megakaryocyte proplatelets. *J. Clin. Invest.* 115:3348–3354. http://dx.doi.org/10.1172/JCI26891

Patel-Hett, S., J.L. Richardson, H. Schulze, K. Drabek, N.A. Isaac, K. Hoffmeister, R.A. Shivdasani, J.C. Bulinski, N. Galjart, J.H. Hartwig, and J.E. Italiano Jr. 2008. Visualization of microtubule growth in living platelets reveals a dynamic marginal band with multiple microtubules. *Blood*. 111:4605–4616. http://dx.doi.org/10.1182/blood-2007-10-118844

Rider, P., Y. Carmi, O. Guttman, A. Braiman, I. Cohen, E. Voronov, M.R. White, C.A. Dinarello, and R.N. Apte. 2011. IL-1α and IL-1β recruit different myeloid cells and promote different stages of sterile inflammation. *J. Immunol.* 187:4835–4843. http://dx.doi.org/10.4049/jimmunol.1102048

Sanjuan-Pla, A., I.C. Macaulay, C.T. Jensen, P.S. Woll, T.C. Luis, A. Mead, S. Moore, C. Carella, S. Matsuoka, T. Bouriez Jones, et al. 2013. Platelet-biased stem cells reside at the apex of the haematopoietic stem-cell hierarchy. *Nature*. 502:232–236. http://dx.doi.org/10.1038/nature12495

Takayama, N., S. Nishimura, S. Nakamura, T. Shimizu, R. Ohnishi, H. Endo, T. Yamaguchi, M. Otsu, K. Nishimura, M. Nakanishi, et al. 2010. Transient activation of c-MYC expression is critical for efficient platelet generation from human induced pluripotent stem cells. *J. Exp. Med.* 207:2817–2830. http://dx.doi.org/10.1084/jem.20100844

Takizawa, H., S. Nishimura, N. Takayama, A. Oda, H. Nishikii, Y. Morita, S. Kakinuma, S. Yamazaki, S. Okamura, N. Tamura, et al. 2010. Lnk regulates integrin alphaIIbbeta3 outside-in signaling in mouse platelets, leading to stabilization of thrombus development in vivo. *J. Clin. Invest.* 120:179–190. http://dx.doi.org/10.1172/JCI39503

Thon, J.N., and J.E. Italiano. 2010. Platelet formation. *Semin. Hematol.* 47:220–226. http://dx.doi.org/10.1053/j.seminhematol.2010.03.005

Thon, J.N., A. Montalvo, S. Patel-Hett, M.T. Devine, J.L. Richardson, A. Ehrlicher, M.K. Larson, K. Hoffmeister, J.H. Hartwig, and J.E. Italiano Jr. 2010. Cytoskeletal mechanics of proplatelet maturation and platelet release. *J. Cell Biol.* 191:861–874. http://dx.doi.org/10.1083/jcb.201006102

Thon, J.N., H. Macleod, A.J. Begonja, J. Zhu, K.C. Lee, A. Mogilner, J.H. Hartwig, and J.E. Italiano Jr. 2012. Microtubule and cortical forces determine platelet size during vascular platelet production. *Nat. Commun.* 3:852. http://dx.doi.org/10.1038/ncomms1838

Yamamoto, R., Y. Morita, J. Ooehara, S. Hamanaka, M. Onodera, K.L. Rudolph, H. Ema, and H. Nakauchi. 2013. Clonal analysis unveils self-renewing lineage-restricted progenitors generated directly from hematopoietic stem cells. *Cell*. 154:1112–1126. http://dx.doi.org/10.1016/j.cell.2013.08.007

Yang, M., K. Li, C.M. Chui, P.M. Yuen, P.K. Chan, C.K. Chuen, C.K. Li, and T.F. Fok. 2000. Expression of interleukin (IL) 1 type I and type II receptors in megakaryocytic cells and enhancing effects of IL-1beta on megakaryocytopoiesis and NF-E2 expression. *Br. J. Haematol.* 111:371–380. http://dx.doi.org/10.1046/j.1365-2141.2000.02340.x

Zhang, L., M. Orban, M. Lorenz, V. Barocke, D. Braun, N. Urtz, C. Schulz, M.L. von Brühl, A. Tirniceriu, F. Gaertner, et al. 2012. A novel role of sphingosine 1-phosphate receptor S1pr1 in mouse thrombopoiesis. *J. Exp. Med.* 209:2165–2181. http://dx.doi.org/10.1084/jem.20121090